



Modeling and Optimization of Rectangular Latent Heat Storage Elements in an Air-Guided Heat Storage System

Matti Grabo, Christoph Staggenborg, Kai Alexander Philippi and Eugeny Y. Kenig*

Chair of Fluid Process Engineering, Faculty of Mechanical Engineering, Paderborn University, Paderborn, Germany

OPEN ACCESS

Edited by:

Theodoros Damartzis,
École Polytechnique Fédérale de
Lausanne, Switzerland

Reviewed by:

Gerhard Schmitz,
Hamburg University of Technology,
Germany
Amin Ghobeily,
Sheridan College, Canada

*Correspondence:

Eugeny Y. Kenig
eugeny.kenig@upb.de

Specialty section:

This article was submitted to Process
and Energy Systems Engineering,
a section of the journal
Frontiers in Energy Research

Received: 11 June 2020

Accepted: 31 August 2020

Published: 09 October 2020

Citation:

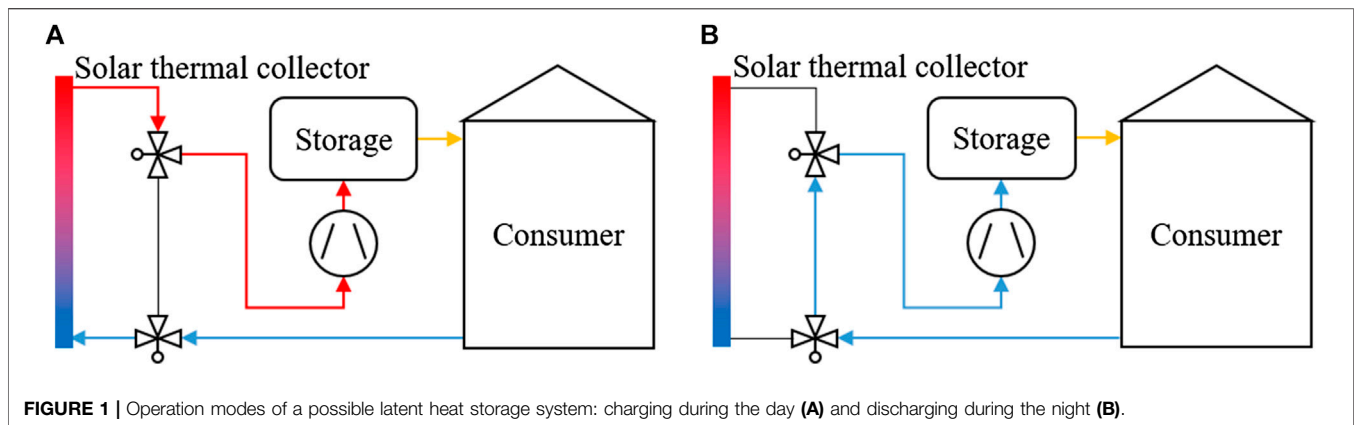
Grabo M, Staggenborg C, Philippi KA
and Kenig EY (2020) Modeling and
Optimization of Rectangular Latent
Heat Storage Elements in an Air-
Guided Heat Storage System.
Front. Energy Res. 8:571787.
doi: 10.3389/fenrg.2020.571787

The thermal performance of macro-encapsulated latent heat storage elements in form of thin, rectangular plates within an air-driven heat storage system is investigated. The plates are made of high-density polyethylene and filled with phase change material. Several plates are stacked together and inserted into a box which can be installed in a heating/air conditioning system. First, an experimental test rig was designed. Measured temperature and pressure drop data retrieved from the rig was then used to validate a simplified computational fluid dynamics model describing a section of the test set-up including a stack of ten plates. Afterward, the model was reduced in complexity in order to perform a parametric study by varying geometric parameters of the storage plates. In total, 217 different geometries were simulated and their thermo-hydraulic efficiency was evaluated. As a result, geometries were proposed, which can potentially increase the thermo-hydraulic efficiency of the storage plates by over 50%.

Keywords: heat transfer, latent heat, heat storage, computational fluid dynamics, phase change material

INTRODUCTION

As reported by the International Energy Agency, only 10% of the global heat production was covered by renewable energy sources in 2018 (International Energy Agency, 2019). One of the ways toward increasing the usability of renewable energies is to adapt the supply of heating and cooling to the current demand and to minimize the cost-intensive consumption of electricity and fossil fuels. Among others, this can be achieved by using heat and cold storages, which increasingly have become a major focus of the heating, ventilation and air conditioning (HVAC) sector. One of the available heat storage technologies are latent heat storages, which use the phase change energy of the storage material and, compared to sensible heat storages, significantly increase the volume-specific storage capacity over a relatively small temperature interval. Materials used in latent heat storage systems are usually referred to as phase change materials (PCM). A typical application of such heat storages can be an air-conditioning system powered by a solar thermal collector, as illustrated in **Figure 1**. The system is charged during the day, when the thermal solar collector heats up an air flow, which is guided through the storage causing the PCM to melt. After leaving the storage, the air has the temperature of the PCM melting point and is distributed to the consumer. During the night, colder air can be pumped through the storage, which causes the PCM to solidify while heating up the air flow to the PCM melting point. Altogether, if properly designed, such a system is able to keep a constant indoor temperature.



In literature, studies of different latent heat storage systems, both experimental and numerical, can be found. Types of latent heat storage include shell-and-tube heat exchangers or direct contact designs as well as packed bed storage tanks. The latter were investigated, among others, by Saitoh and Hirose (1986), Ismail and Henríquez (2002), and Loem et al. (2019). In such systems, the PCM capsules are randomly packed in a tank, and a heat transfer fluid releases heat to the bed while charging or extracts heat while discharging. Storages of structured PCM element arrangements were, for example, described by Darzi et al. (2013). In their numerical study, rectangular, plane PCM plates were used and the influence of operational parameters, such as mass flow rate and inlet temperature, as well as geometrical parameters, such as plate thickness, was investigated. Darzi et al. (2013) found that the plate thickness linearly correlates with the melting duration. Gowreesunker et al. (2013) studied the performance of a PCM plate heat exchanger for air-conditioning of an airport terminal building by using a coupled numerical model. They found that the cooling and partially the heating efforts can be reduced by using PCM and that energy savings of more than 30% can be achieved. The plate encapsulation used in their work was metallic and had surface extensions in form of pin fins in order to increase heat transfer. A recent study of a system consisting of in-duct PCM plates of the same type as used by Gowreesunker et al. (2013) was published by Kumirai et al. (2019). They varied operational parameters, such as inflow velocity and temperature, and compared different PCM in terms of thermal effectiveness. A similar rectangular plate design was investigated by Larrinaga et al. (2020) who investigated the effect of the arrangement of the plate stacks. They found that higher mass flow rates reduce the charging and discharging duration of the storage and that arranging plate stacks in series increases the duration.

Since the performance of the heat storage depends on the ability of the storage elements to effectively transfer energy to the heat transfer fluid, the focus of this study was laid on the design and optimization of new PCM heat storage plates similar to those investigated in the last three studies mentioned above. A new plate design was introduced, which had surface extensions in form of a square based pyramid. The encapsulation material of this plate was high-density polyethylene (HDPE) and the PCM was a salt hydrate. In practice, these plates are stacked and

inserted into a box, which has connecting fittings for the installation in air ducts. The plates and the storage box are illustrated in **Figure 2**. Further, a test rig was set-up in order to evaluate the thermal and pressure drop performance of the plates. Based on the experimental setup, a computational fluid dynamics (CFD) model was developed and validated. Next, this model was reduced in complexity in order to perform a parametric study with respect to several geometry parameters of the plate.

METHODS

As can be seen in **Figure 2**, the PCM plates were designed with an extended surface in the form of a pyramidal frustum. The dimensions of the frustum are 15 mm by 15 mm on the base; the frustum height is 3 mm. The angle between the frustum side faces and the base area is 30°. It should be noted, that the thickness of the plate is constant, which means that the bulges on the top side have similar indentations on the bottom side. The overall thickness of the plate is 5 mm, while the HDPE capsule wall is 1 mm thick, thus resulting in a PCM layer thickness of 3 mm. The PCM volume per plate is around 100 ml. The plates can be stacked up to a variable number, and multiple stacks can be inserted into the container allowing for a variable storage capacity. In order to allow for an improved charging/discharging rate, the surface extensions of the plates were evaluated with the help of CFD.

Experimental

A test rig illustrated in **Figure 3** was set-up in order to acquire data for the validation of numerical results. It comprised a duct, in which a stack of ten PCM plates was inserted. Dry air was pumped through the duct by a compressor, then heated and straightened by a filter element before entering the stack. Temperatures were measured with six PT100 class-A sensors with an accuracy of 0.35 K. Two sensors were installed upstream and four sensors downstream of the plate stack in order to determine the thermal performance of the plates under varying inflow temperatures T_{in} . The temperature sensors were evenly distributed within the cross-section of the duct. The

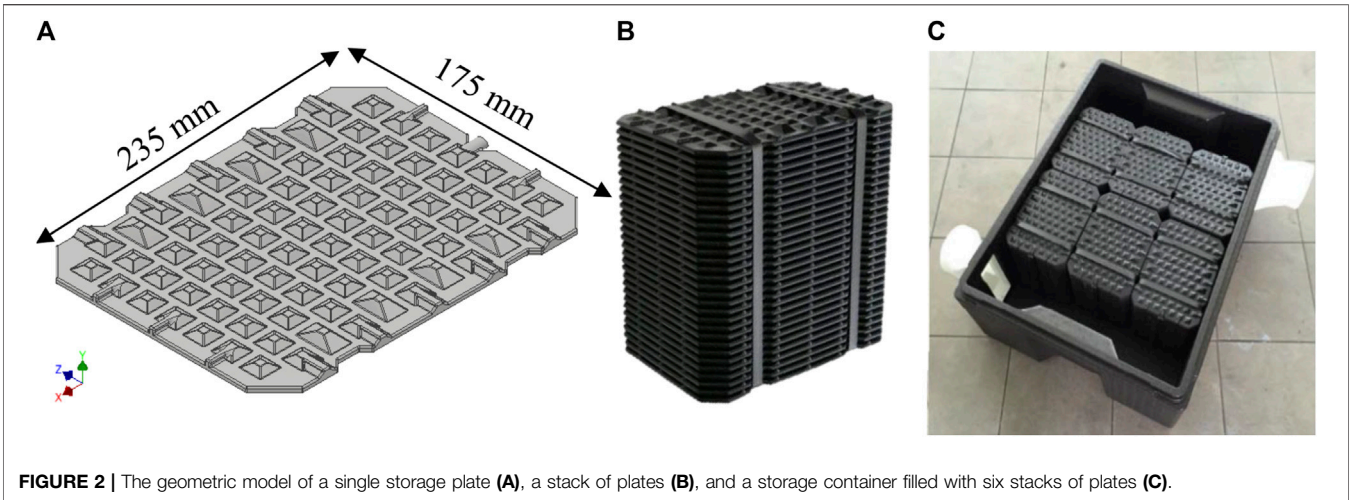


FIGURE 2 | The geometric model of a single storage plate (A), a stack of plates (B), and a storage container filled with six stacks of plates (C).

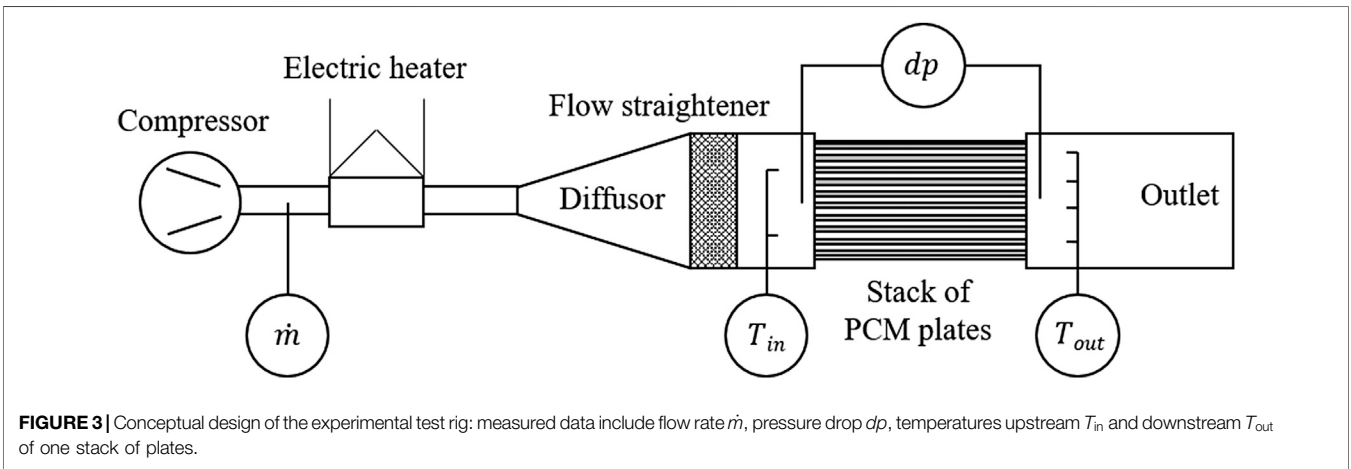


FIGURE 3 | Conceptual design of the experimental test rig: measured data include flow rate \dot{m} , pressure drop dp , temperatures upstream T_{in} and downstream T_{out} of one stack of plates.

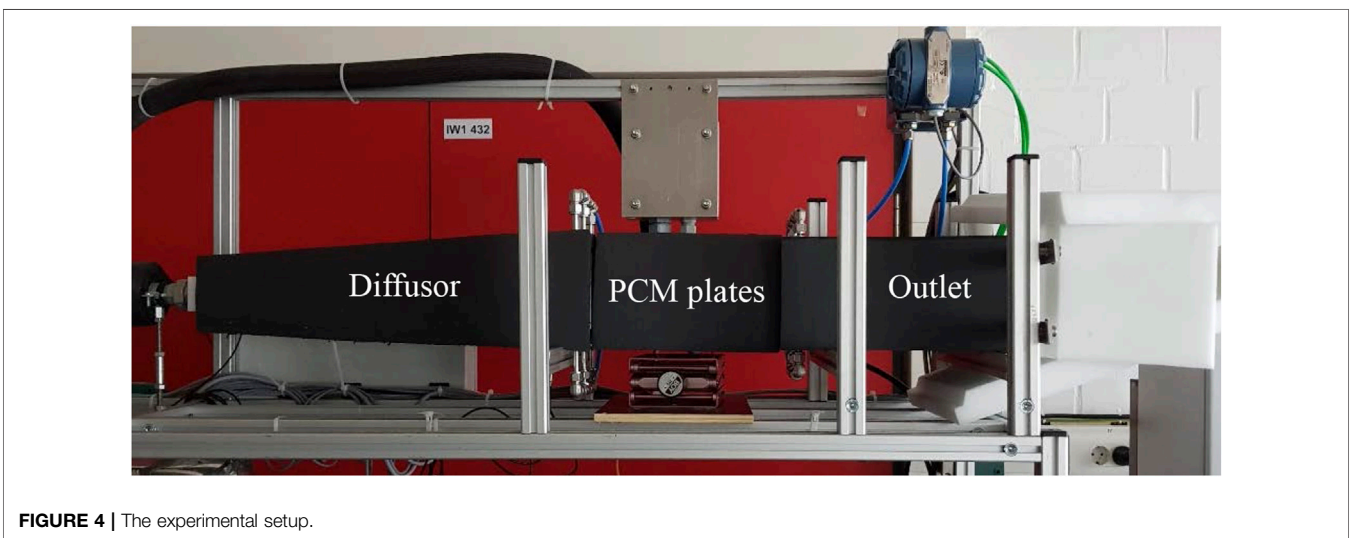


FIGURE 4 | The experimental setup.

TABLE 1 | Properties of PCM and HDPE.

	PCM	HDPE
Density (kg/m ³)	1,300	945
Specific heat capacity [J/(kgK)]	2,000	1,845
Thermal conductivity [W/(mK)]	0.6	0.4
Thickness (mm)	3	1
Latent heat of fusion (kJ/kg)	220	—

PCM, phase change material; HDPE, high-density polyethylene.

pressure drop dp was measured with a Rosemount 3051S1CD differential pressure flow transmitter with 0.09% span accuracy. A Brooks 5853S mass flow controller with an accuracy of 0.7% was located between the compressor and the heater in order to control the incoming flow. To minimize ambient temperature influence, the whole setup was insulated with ArmaFlex elastomeric foam. A photograph of the experimental setup is shown in **Figure 4**. Experiments were carried out with flow rates of 150, 275, and 400 L/min and inlet temperatures of 35 and 39°C for melting and 25°C for solidification. The Reynolds numbers $Re = \rho u d_h / \mu$ within the channels for the highest volumetric flow rate were around 560 corresponding to an average flow velocity u of 1.6 m/s. Here, ρ and μ denote density and dynamic viscosity of air, respectively. The hydraulic diameter $d_h = 4A_c/P$ was calculated from the cross-sectional area A_c of a channel between two plates and the wetted perimeter P of such a channel. For the inlet region, Reynolds numbers around 3,800 were obtained.

The PCM used was the salt hydrate ATS30 by the manufacturer Axiotherm GmbH, with a solidus temperature $T_s = 28^\circ\text{C}$ and a liquidus temperature $T_l = 33^\circ\text{C}$ for melting and $T_s = 27^\circ\text{C}$ and $T_l = 30^\circ\text{C}$ for solidification (Axiotherm, 2020). The encapsulation material was HDPE. The properties of the PCM and HDPE are given in **Table 1**. **Figure 5** shows the partial enthalpy distribution of the used PCM provided by the manufacturer.

Computational Fluid Dynamics Model of the Test Rig

In order to optimize the plate design, a simplified CFD model of the air duct containing the plate stack was developed. The simulation tool used to implement the model was STAR-CCM+ 13.04. Due to the symmetry of the plates, only a thin slice section in the center of the stack was modeled, which enabled a significant reduction of the computational effort. The CFD model is illustrated in **Figure 6**.

The computational model consisted of two domains: air and PCM. The thickness of the capsule walls was not explicitly resolved, rather it was accounted for by applying a thermal resistance at the boundary that separates the air and the PCM. The thermal resistance was determined from the thickness and the thermal conductivity of the HDPE capsule walls (**Table 1**). At the air inlet, a constant mass flow rate and a specific temperature was defined. Assuming a perfect thermal insulation of the duct, the top and bottom sides were considered as adiabatic, with a no-slip boundary condition. The left and right side of the computational domain were described by symmetry boundary conditions, as shown in **Figure 6**. At the outlet, zero-gradient boundary conditions for pressure and temperature were applied. Note that due to the particular installation of the plate stack on the test rigs, three channels were blocked, as indicated in **Figure 6**. In order to properly attach the plates to the test rig, a special console had to be designed, which contained a stack of 10 plates. Since some part of the cross-sectional area of the stack was covered by the console, one plate was removed in the simulation, because no circulation around this plate was expected. However, during the installation of the test rig, it became clear, that more than just one plate was covered by the console. This was accounted for in the model by closing another channel at the top.

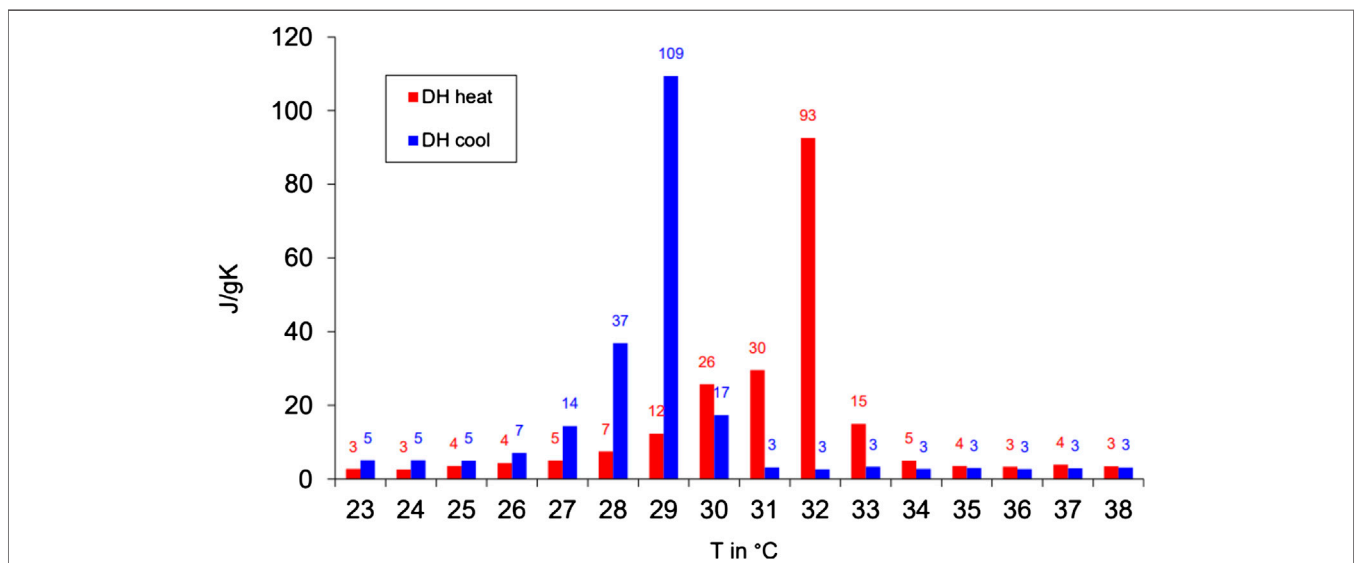


FIGURE 5 | Partial enthalpy distribution of the phase change material ATS30 (Axiotherm, 2020).

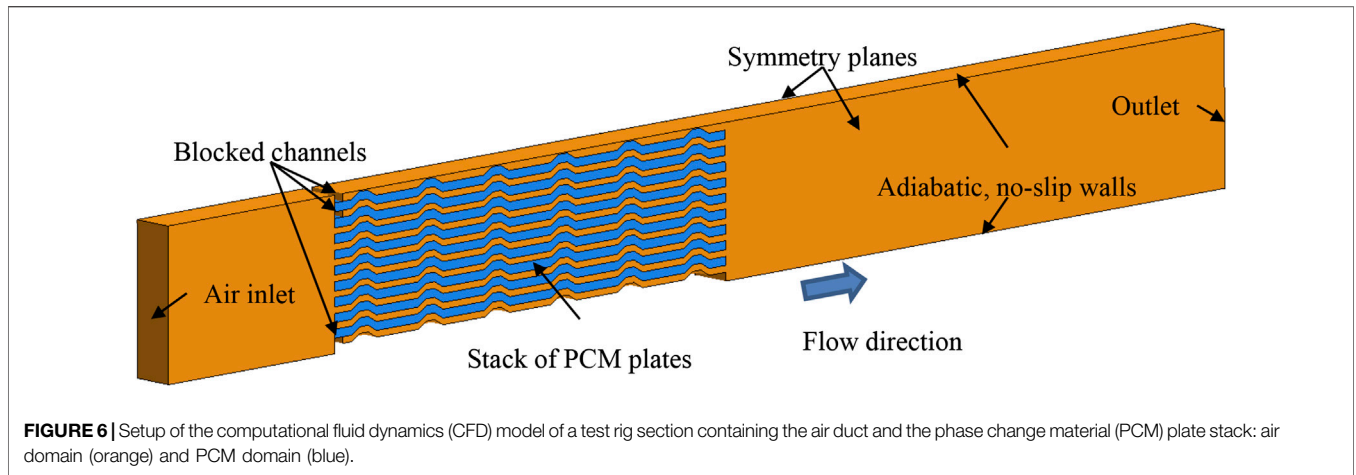


FIGURE 6 | Setup of the computational fluid dynamics (CFD) model of a test rig section containing the air duct and the phase change material (PCM) plate stack: air domain (orange) and PCM domain (blue).

Due to relatively low flow velocities, the Mach number was not expected to exceed 0.3. Therefore, the air flow was assumed to be incompressible and modeled by the following governing equations:

$$\frac{\partial u}{\partial t} + (u \cdot \nabla)u = -\nabla p + \mu \Delta u \quad (1)$$

$$\nabla \cdot u = 0 \quad (2)$$

Heat transport was described by the energy equation:

$$\frac{\partial T}{\partial t} + \nabla \cdot (uT) = a \nabla^2 T \quad (3)$$

Here, u denotes velocity, t time, p pressure field, μ dynamic viscosity, T temperature and a thermal diffusivity. Turbulence was modeled using an extended version of the $k-\epsilon$ model, namely, the elliptic blending model by Billard and Laurence (2012), which is suggested for internal flows involving heat transfer at moderate Reynolds numbers. For the heat transfer inside the plates, it was assumed that, due to the low thickness and high viscosity of the liquid PCM, only heat conduction takes place and any type of convection can be neglected. The phase change process was described using the following equation:

$$\rho c_p \frac{\partial T}{\partial t} = k \nabla^2 T - \rho L \frac{\partial \gamma}{\partial t} \quad (4)$$

The thermal conductivity k , the density ρ and the specific heat capacity c_p were assumed to be constant. L denotes the latent heat of fusion. The liquid fraction of the PCM γ is usually a function of temperature (Voller and Swaminathan, 1991). In this work, a linear $\gamma-T$ relation was applied:

$$\gamma = \begin{cases} 0 & T < T_s \\ \frac{T - T_s}{T_l - T_s} & T_s \leq T \leq T_l \\ 1 & T > T_l \end{cases} \quad (5)$$

Meshing was performed with polyhedral elements and prism layers near the walls. A grid independence study yielded a mesh element size of 0.1 mm and a time step of 0.5 s as sufficient. Multiple

simulations were carried out with flow rates of 150, 275, and 400 L/min. As inlet temperature, the measured inlet temperature curves were used. The temperature and pressure drop were evaluated at the same positions as on the real test rig, upstream and downstream of the plate stack. The simulated outlet temperatures and pressure drops were compared to the measured data.

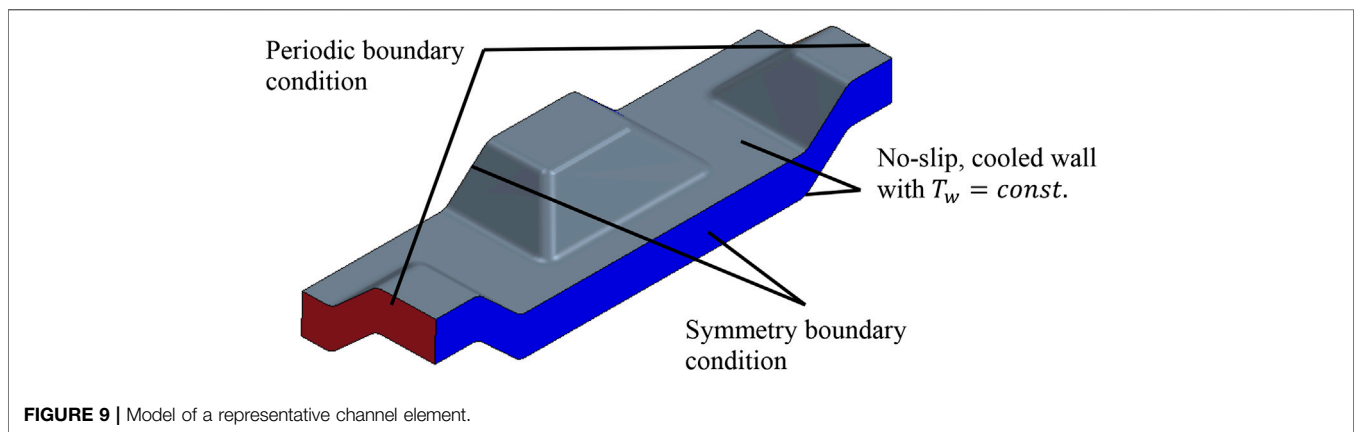
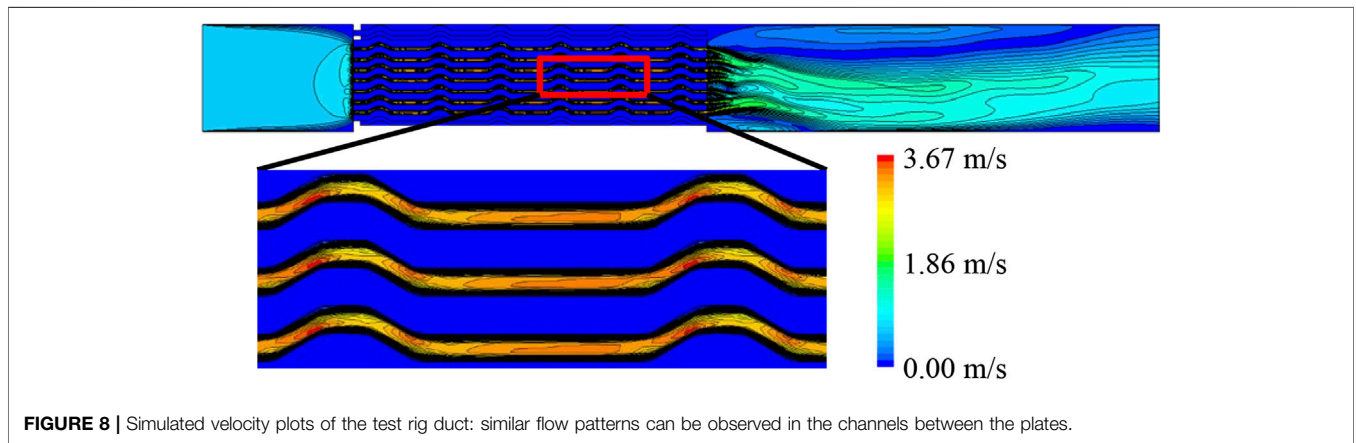
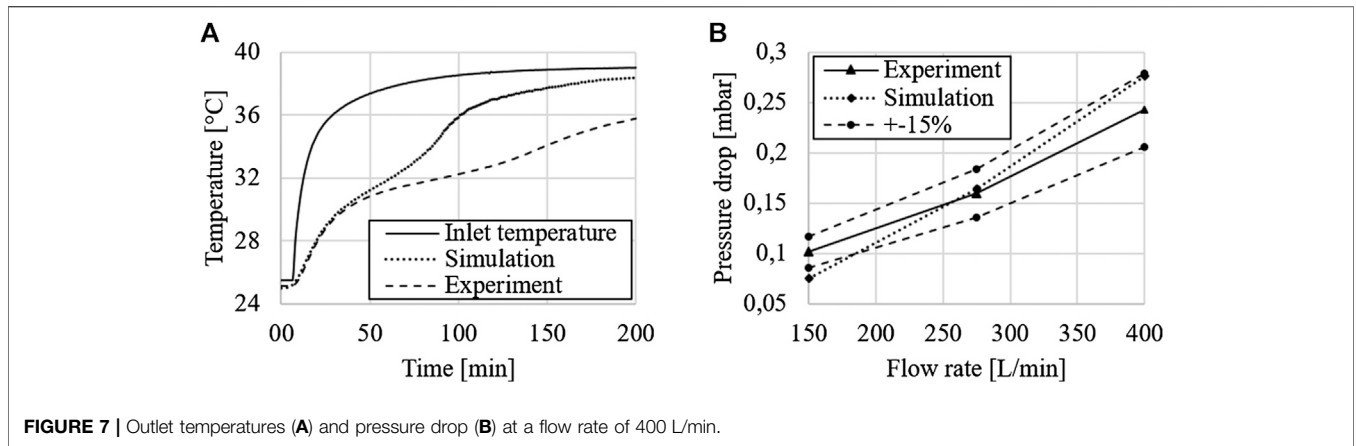
As can be seen in Figure 7, the simulated outlet temperatures deviate strongly from the measured ones, especially after the start of the phase change process at approximately 50 min. A possible explanation is the thermal mass of the test rig components, such as the diffusor, duct, outlet, etc., which could not be considered in the CFD model. Besides, by simulating only a slice section of the duct geometry, side effects were neglected. Further, the model assumed a perfectly insulated duct, and hence, heat losses to the environment were neglected. These effects lead to a much slower temperature rise in the experiments. Based on these results, we can conclude that it is not practical to model the actual heat transport within the duct. However, the simulated and measured pressure drop values are in good agreement, which indicates that the flow phenomena within the duct are properly captured.

Representative Element for Parametric Study

The simulated flow distribution is shown in Figure 8. It can be seen that the flow pattern inside the individual channels between two plates is similar. This similarity can be used to reduce the initial computational domain to a small representative element.

This element was used to perform a parametric study to identify optimized plate geometries with increased heat transfer and/or lower pressure drop compared to the original design. The model of the representative element, which has the dimensions 10 mm by 40 mm, is illustrated in Figure 9.

The phase change phenomena inside the PCM were not modeled, since the actual heat transport into the capsule as well as the pressure drop entirely depend on the actual shape of the capsule surface and operational parameters, such as air flow velocity or inlet temperature. This allows to consider the air flow as steady-state and evaluate the pressure drop and heat transfer



under steady-state conditions. By applying a periodic boundary condition at the inlet and outlet of the element, this steady-state was enforced. The wall temperature T_w was kept constant at 20°C, the inflow velocity u was set to 3 m/s and the inlet temperature to 30°C. The mesh consisted of polyhedral cells in the bulk flow and prism layers near the walls. After performing a grid independence study of the representative element, a mesh element size of 0.15 mm was chosen.

Comparing the pressure drop over the representative element with that in equivalent sections of the duct model, only small differences (<10%) were found, which indicates that the element represents the whole duct model reasonably well and can be used for a parametric study.

In this study, different plate surface geometries were created and evaluated based on their thermo-hydraulic efficiency ϵ , which is the ratio of the heat transferred through the element wall and

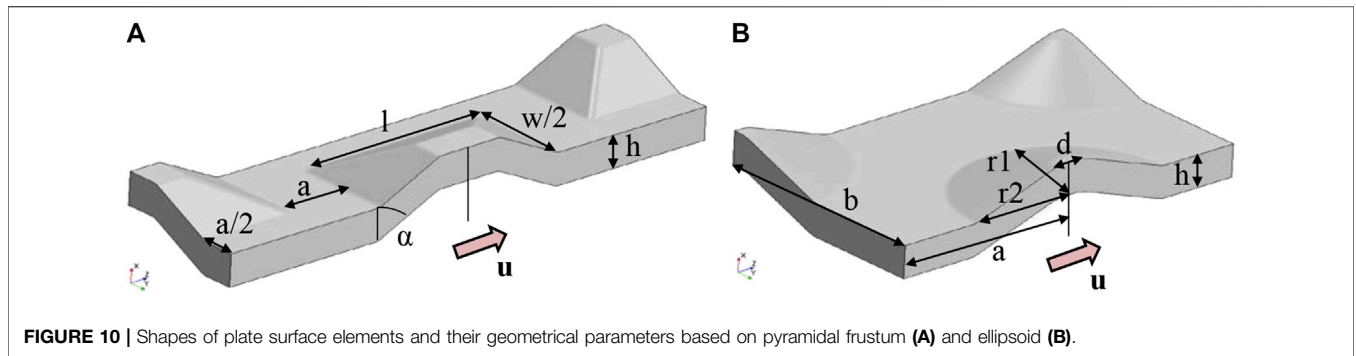


FIGURE 10 | Shapes of plate surface elements and their geometrical parameters based on pyramidal frustum **(A)** and ellipsoid **(B)**.

the pumping effort (Eq. 6). This criterion was used before by, for example, Mitrovic and Maletic (2011) for the evaluation of pillow plate heat exchangers.

$$\varepsilon = \frac{A_w \dot{q}_w}{u_{in} A_{ce} \Delta p} \quad (6)$$

In Eq. 6, A_w denotes the wetted wall area of the element, \dot{q}_w is the heat flux through the wall, u_{in} is the inlet flow velocity, A_{ce} is the cross-sectional area of the element and Δp is the pressure drop across the element. The thermo-hydraulic efficiency was determined for all considered geometries and then compared to ε_{ref} , which represents the thermo-hydraulic efficiency of the

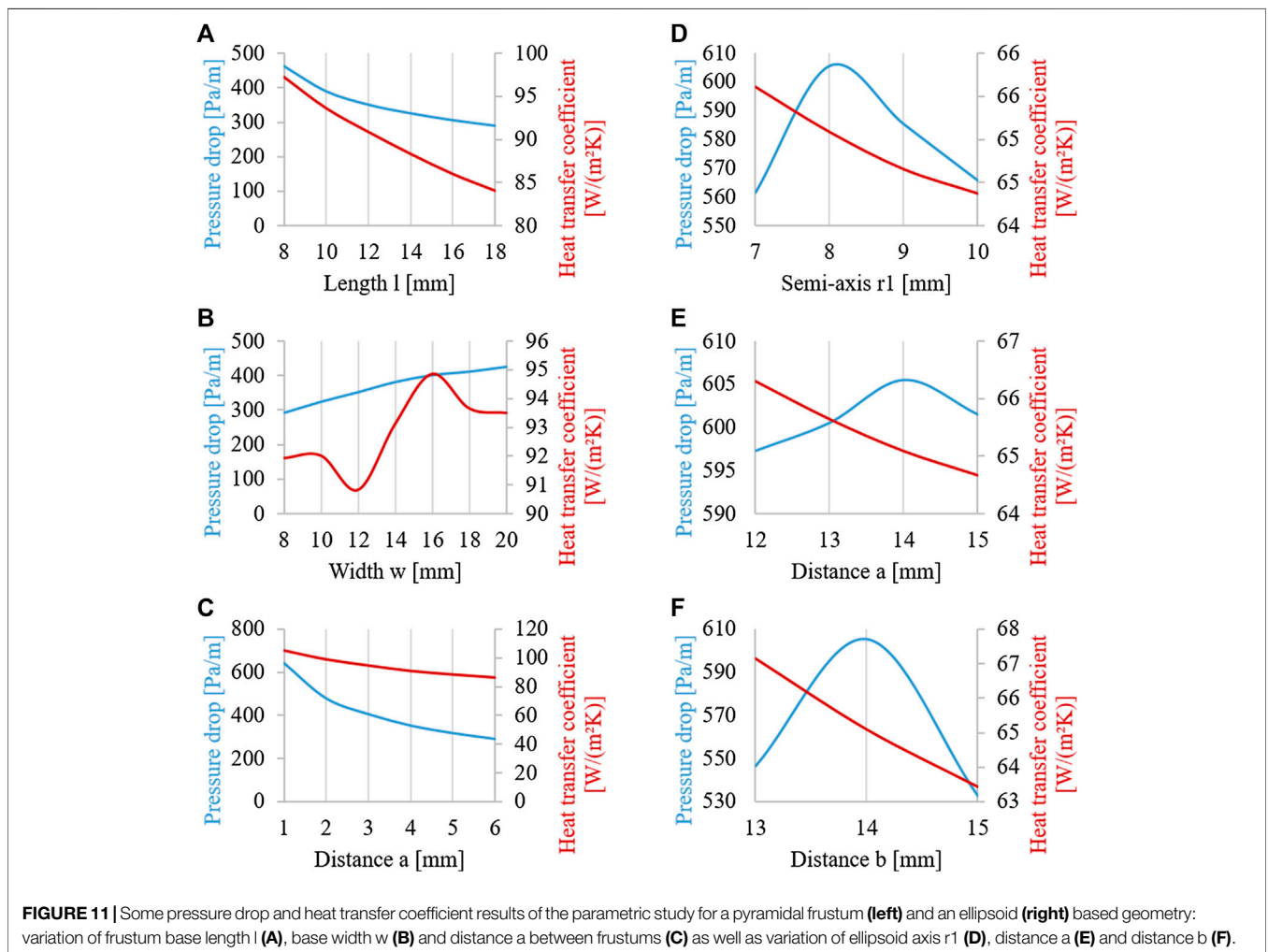


FIGURE 11 | Some pressure drop and heat transfer coefficient results of the parametric study for a pyramidal frustum (left) and an ellipsoid (right) based geometry: variation of frustum base length **(A)**, base width **(B)** and distance **a** between frustums **(C)** as well as variation of ellipsoid axis **r1** **(D)**, distance **a** **(E)** and distance **b** **(F)**.

original geometry. The ratio $\varepsilon/\varepsilon_{\text{ref}}$ evaluates the relative improvement or worsening of the respective geometry. Multiple geometry parameters were changed in the course of the study, which are shown in **Figure 10**. The original geometry was based on a square pyramidal frustum. The shape of the frustums as well as their arrangement and the height of the channel were varied. Further, an ellipsoid based geometry was investigated, for which the length of the minor and major axis, the arrangement of the elliptic elements and the channel height were varied. In total, 217 different geometry variations were tested and compared to the original geometry.

RESULTS

The influence of some investigated geometrical parameters is shown at the left of **Figure 11** for a frustum reference shape with $l = w = 12 \text{ mm}$, $a = 4 \text{ mm}$, $h = 3 \text{ mm}$ and $\alpha = 45^\circ$. Each parameter was changed, while the other were kept constant. Also, combinations were tested, when more than one parameter was changed attempting to find additional local optima. As can be seen in the plots in **Figure 11**, similar trends in the behavior of both heat transfer coefficient and pressure drop can usually be encountered. For instance, when pressure drop decreases, the heat transfer coefficient decreases as well. However, the slopes are different, and therefore, the optimal compromise between heat transfer and pressure drop can only be found by analyzing the thermo-hydraulic efficiency (Eq. 6). Using this analysis, we found that the frustum based geometries have an improvement potential of only 14% compared to the original.

The same procedure was performed for the ellipsoid based geometries; some illustrative results for a base shape of $a = b = 14 \text{ mm}$, $h = 3 \text{ mm}$, $d = 2 \text{ mm}$, $r_1 = 6 \text{ mm}$ and $r_2 = 8 \text{ mm}$ are shown at the right of **Figure 11**. As can be seen, the ellipsoidal shapes usually show a maximum of pressure drop, while the heat transfer coefficient decreases with higher geometrical dimensions. The reason for this behavior is the lower surface area available for heat transfer, since with increasing distance between the surface

elements, the number of elements per plate decreases. This results in a lower surface area per plate and therefore in reduced heat transfer. The behavior of the pressure drop was somewhat surprising, since we expected its increase together with increasing surface area. However, as can be seen in **Figure 11**, there is a maximum instead. Such a maximum can also be encountered for other combinations of geometry parameters and geometry variants not shown here, which indicates a higher potential of the ellipsoidal shape for increasing the thermo-hydraulic efficiency. This was indeed confirmed after evaluating 126 different geometry variants based on the ellipsoidal shape, when a possible ε improvement of 46% compared to the original geometry was found. Based on the ellipsoidal shape, an alternative, non-symmetric shape in form of a falling droplet was also investigated, while 38 geometry variants were studied and a further improvement of ε up to 52% could be achieved. The optimized droplet geometry is illustrated in **Figure 12**.

CONCLUDING REMARKS

In this work, rectangular, thin heat storage capsules filled with PCM were investigated with respect to their heat transfer performance and pressure drop. The focus was laid on the CFD modeling of the flow and heat transfer in the channels between the plates in order to optimize their shape. Therefore, a test rig was set-up to experimentally evaluate reference plates, and the measured data was used to validate the CFD model of the duct containing a stack of PCM plates. Afterward, the model was reduced in complexity and a representative element was identified, for which a parametric study was performed. Different base geometries were tested as surface extension elements for the storage plates, including pyramidal frustum and ellipsoidal shapes, by changing various geometrical parameters. In total, 217 different geometry variants were simulated and their thermo-hydraulic efficiency was evaluated. Comparing the respective efficiency of each variant with the reference geometry shown in **Figure 2**, a maximal improvement

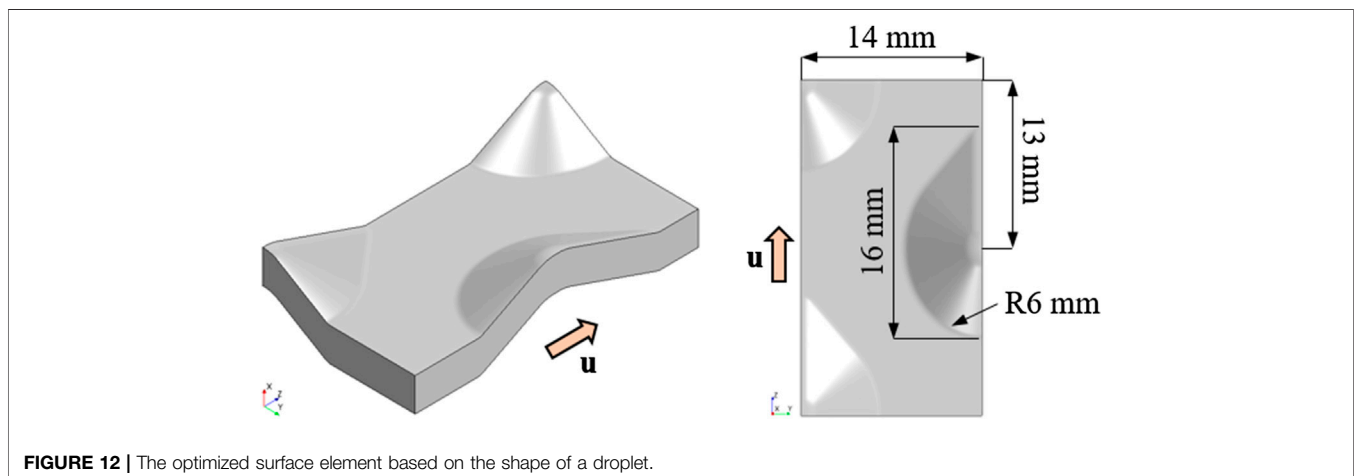


FIGURE 12 | The optimized surface element based on the shape of a droplet.

of 52% was achieved. The optimized shape of surface element based on a droplet shape is shown in **Figure 12**.

The optimized surface geometry of the representative element can be used for the design of improved PCM plates. For an upcoming project, it is planned to manufacture several of these optimized plates together with a consortium partner and to perform further experimental studies. Besides, the storage container in which the plates are stacked will also be investigated to reach further improvement in order to allow for an even flow distribution. Subsequently, future investigations will involve the performance testing of the optimized plates under real operational conditions in a demonstrator building.

DATA AVAILABILITY STATEMENT

All datasets presented in this study are included in the article.

REFERENCES

- Axiotherm GmbH (2020). Data sheet—ATS 30. Available at: <https://www.axiotherm.de/de/download/project/productdatasheet/file/14/> (Accessed August 14, 2020).
- Billard, F., and Laurence, D. (2012). A robust $k-\epsilon-v^2/k$ elliptic blending turbulence model applied to near-wall, separated and buoyant flows. *Int. J. Heat Fluid Flow* 33 (1), 45–58. doi:10.1016/j.ijheatfluidflow.2011.11.003
- Darzi, A. R., Moosania, S. M., Tan, F. L., and Farhadi, M. (2013). Numerical investigation of free-cooling system using plate type PCM storage. *Int. Commun. Heat Mass Transf* 48, 155–163. doi:10.1016/j.icheatmasstransfer.2013.08.025
- Gowreesunker, B. L., Tassou, S. A., and Kolokotroni, M. (2013). Coupled TRNSYS-CFD simulations evaluating the performance of PCM plate heat exchangers in an airport terminal building displacement conditioning system. *Build. Environ* 65, 132–145. doi:10.1016/j.buildenv.2013.04.003
- International Energy Agency (2019). Renewables 2019—market analysis and forecast from 2019 to 2024. Available at <https://www.iea.org/reports/renewables-2019/heat>. (Accessed June 5, 2020).
- Ismail, K. R., and Henriquez, J. R. (2002). Numerical and experimental study of spherical capsules packed bed latent heat storage system. *Appl. Therm. Eng* 22 (15), 1705–1716. doi:10.1016/S1359-4311(02)00080-7
- Kumirai, T., Dirker, J., and Meyer, J. (2019). Experimental analysis for thermal storage performance of three types of plate encapsulated phase change materials in air heat exchangers for ventilation applications. *J. Build. Eng* 22, 75–89. doi:10.1016/j.jobbe.2018.11.016
- Larrinaga, P., Diarce, G., Campos-Celador, A., and García-Romero, A. (2020). Parametric characterization of a full-scale plate-based latent heat thermal energy storage system. *Appl. Therm. Eng* 178, 115441. doi:10.1016/j.applthermaleng.2020.115441
- Loem, S., Deethayat, T., Asanakham, A., and Kiatsiroat, T. (2019). Thermal characteristics on melting/solidification of low temperature PCM balls packed bed with air charging/discharging. *Case Stud. Therm. Eng* 14, 100431. doi:10.1016/j.csite.2019.100431
- Mitrovic, J., and Maletic, B. (2011). Numerical simulation of fluid flow and heat transfer in thermoplates. *Chem. Eng. Technol* 34 (9), 1439–1448. doi:10.1002/ceat.201100271
- Saitoh, T., and Hirose, K. (1986). High-performance phase-change thermal energy storage using spherical capsules. *Chem. Eng. Commun* 41 (1–6), 39–58. doi:10.1080/00986448608911711
- Voller, V. R., and Swaminathan, C. R. (1991). General source-based method for solidification phase change. *Numer. Heat Trans. B* 19 (2), 175–189. doi:10.1080/10407799108944962

AUTHOR CONTRIBUTIONS

All authors listed have made a substantial, direct and intellectual contribution to the work, and approved it for publication.

FUNDING

The authors are grateful to the German Federal Ministry of Economic Affairs and Energy for their financial support of the project “MoLaWS: Development of a modular heat storage system using high-capacity, innovative latent heat storage elements” (Reference Number: ZF4032917ST7).

ACKNOWLEDGMENTS

Calculations leading to the results presented here were performed on resources provided by the Paderborn Center for Parallel Computing.

Conflict of Interest: The remaining authors declare that the research was conducted in the absence of any commercial or financial relationships that could be construed as a potential conflict of interest.

Copyright © 2020 Grabo, Staggenborg, Philippi and Kenig. This is an open-access article distributed under the terms of the Creative Commons Attribution License (CC BY). The use, distribution or reproduction in other forums is permitted, provided the original author(s) and the copyright owner(s) are credited and that the original publication in this journal is cited, in accordance with accepted academic practice. No use, distribution or reproduction is permitted which does not comply with these terms.